

# FREEZING-THAWING ASSISTED SYNTHESIS OF NOVEL CARRAGEENAN NANOMAGNETIC BEADS FOR CONTROLLED RELEASE OF ANTITUMOR DRUGS

HOSSEIN HOSSEINZADEH

*Department of Chemistry, Payame Noor University, 19395-4697, Tehran, Iran*

✉ *Corresponding author: HosseinHosseinzadeh,h\_hoseinzadeh@pnu.ac.ir*

*Received* May 26, 2015

In this study, a new series of magnetic responsive beads (MRBs), as nanocarriers for effective controlled release of doxorubicin (DOX) antitumor drug, were prepared using a simple freezing-thawing method. The synthesized MRBs have a magnetic core surrounded by a shell comprising a  $\text{Ca}^{2+}$ -crosslinked *kappa*-carrageenan/poly(vinyl alcohol) composite. The structural, morphological and magnetic properties of the MRBs were characterized by Fourier transform infrared spectroscopy (FTIR), scanning electron microscopy (SEM), transmission electron microscopy (TEM), X-Ray diffraction (XRD), and vibrating sample magnetometry (VSM). DOX was then successfully loaded into the MRB nanocarriers. Moreover, the *in vitro* release of DOX was studied at different pH values and in the presence of an external magnetic field. The release curves were well-fitted by the Korsmeyer-Peppas equation with a non-Fickian diffusion mechanism. The results indicate that the prepared novel MRBs can serve as promising platforms to the synthesis of magnetic targeted drug delivery systems.

**Keywords:** nanomagnetic, *kappa*-carrageenan, beads, controlled release, antitumor drugs

## INTRODUCTION

Nowadays, a wide range of nanocarriers have been designed for drug delivery systems (DDS).<sup>1-4</sup> Among them, magnetic nanoparticles (MNPs) have received much attention in developing targeted drug delivery systems (DDS) due to their unique properties.<sup>5-9</sup> In particular, magnetic iron oxide nanoparticles (MIONs) have been recently coated chemically or physically with various polymer matrixes.<sup>10-14</sup> Up to now, three main strategies have been suggested to synthesize and incorporate the MIONs into crosslinked polymer networks.<sup>15</sup> The "network first" and the "MIONs first" are two commonly used methods, in which preformed polymeric network or presynthesized MIONs are mixed with an aqueous solution of iron salts and or into a polymer matrix, respectively.<sup>16-18</sup> These methods, however, have serious disadvantages, mainly the instability and aggregation of MIONs. In the third method, the aqueous solution of polymer and iron salts is added dropwise into an alkaline solution for the

simultaneous and *in situ* formation of MIONs and cross-linked polymer network.<sup>12,19</sup> This method is facile, effective and convenient for the preparation of MION/polymer networks.

In this contribution, we incorporate the MIONs into two biodegradable, water-soluble and inexpensive polymers, *i.e.* *kappa*-carrageenan and poly(vinyl alcohol), followed by their physical cross-linking with freezing-thawing treatment and  $\text{Ca}^{2+}$  cations. Carrageenans are linear sulfate polysaccharides that are obtained by extraction from certain edible species of red seaweeds.<sup>20</sup> Due to their exceptional properties, carrageenans are widely used as ingredients in a variety of applications. Since carrageenan is a highly negatively charged macromolecule, it can interact with any species carrying a positive charge. Many reports are published in this regard, investigating the interaction of carrageenan with univalent and divalent cations,<sup>21</sup> gelatin,<sup>22</sup> and chitosan.<sup>23</sup>

Poly(vinyl alcohol) (PVA) has been extensively used in many biomaterial applications due to the characteristics of easy preparation, good biodegradability, excellent chemical resistance, good mechanical properties, processability and good chemical resistance.<sup>24</sup>

In addition, because of the strong hydrophilic and hydrogen bonding character of PVA, it can form new materials, which can be applied in medicine and the pharmaceutical industry.<sup>24</sup> However, its low gel strength, poor mechanical reliability and low fracture toughness have limited its application. Since *kappa*-carrageenan contains high contents of sulfate and hydroxyl functional groups, it may potentially be miscible with PVA due to the formation of hydrogen bonds.

Although various beads based on carrageenan and poly(vinyl alcohol) were obtained,<sup>25-27</sup> the preparation of magnetic carrageenan/PVA hydrogel beads for drug delivery has not yet been studied. Therefore, following a continuous research on carrageenan modification,<sup>28-31</sup> we attempted in this work to prepare *kappa*-carrageenan/PVA blends and analyze their antitumor drug loading and releasing behaviors.

## EXPERIMENTAL

### Materials

The polysaccharide, *kappa*-carrageenan ( $\kappa$ C, from Condinson Co., Denmark), poly(vinyl alcohol) (degree of hydrolysis 99%, MW 89,000-98,000, from Aldrich Chemicals), ferric chloride hexahydrate ( $\text{FeCl}_3 \cdot 6\text{H}_2\text{O}$ , from Merck), ferrous chloride tetrahydrate ( $\text{FeCl}_2 \cdot 4\text{H}_2\text{O}$ , from Merck) and doxorubicin hydrochloride (DOX.HCl, from JaberebneHayan Pharmaceutical Co., Tehran, Iran) were of analytical grade and used without further purification.

### Preparation of beads

The magnetic responsive beads (MRBs) containing MIONs were synthesized by a facile method, *via* the coprecipitation of iron ions in alkaline solution. So, based on this method, a green procedure for synthesis of MRBs was conducted as follows: 1.0 g of PVA was firstly dispersed in 50 mL of doubly distilled water at 70 °C for 30 min. After complete dissolution of PVA, 1.0 g of  $\kappa$ C was added to the solution. After cooling the solution, appropriate amounts of  $\text{FeCl}_2 \cdot 4\text{H}_2\text{O}$  (2.0 g) and  $\text{FeCl}_3 \cdot 6\text{H}_2\text{O}$  (4.0 g) were added into the solution. The mixture was dispersed in duplicate using a 750 Watt ultrasonic processor. Then, the mixture was gradually dropped into 20 mL of 2M  $\text{NH}_4\text{OH}$  and 0.2 M  $\text{CaCl}_2$  solution with vigorous stirring for 60 min. Finally, five freezing-thawing cycles were utilized to prepare magnetic  $\kappa$ C/PVA beads. The product was cut into small pieces and was dried at room temperature.

### Drug loading

The DOX loading onto the MRBs was carried out by immersing 20 mg of powdered sample with average particle sizes between 250-350  $\mu\text{m}$  in 3 mL of DOX.HCl solution with various concentrations (0.5-4.0 mg/mL). The mixture was shaken at a rate of 200 rpm at 37 °C in a rotary shaker for 30 min. The drug loaded MRBs were collected by magnetic separation and then washed several times with phosphate buffer solution (pH=7.4) to remove any surface-adsorbed drug and then air-dried. The percentage of DOX loading efficiency (LE%) was measured using UV-Vis spectrophotometry at 479 nm and according to Eq. 1:<sup>32</sup>

$$LE\% = \frac{\text{amount of DOX added}}{\text{amount of MRB}} \times 100 \quad (1)$$

### Drug release

The dried DOX loaded MRBs (20 mg) were suspended in 3 mL of buffer solutions (pH=2.0 and 7.0). The dissolution medium was placed on a rotary shaker at 37 °C with continuous stirring at 100 rpm. Aliquots (0.5 mL) were withdrawn periodically to determine drug concentration and, in all cases, equal volumes of dissolution media were immediately added to maintain a constant volume. The cumulative amount of DOX released into the solution was determined with a UV-Vis spectrophotometer at 479 nm. The amount of DOX released from the MRBs in the dissolution media was calculated by using previously established calibration standard curves (absorbance as a function of time) of drug in the corresponding buffer and expressed as percentage of the total drug content of the investigated samples. Experiments were performed in triplicate, and the average value was considered for the purposes of data treatment and plotting. The drug release percent was calculated using the following equation:

$$\text{Released drug (\%)} = \frac{R_t}{L} \times 100 \quad (2)$$

where  $L$  and  $R_t$  represent the initial amount of drug loaded and the final amount of drug released at time  $t$ .

### Instrumentation

Fourier transform infrared (FTIR) spectra of samples in KBr pellets were taken, using an FTIR spectrophotometer (Bruker, Germany) at room temperature. The surface morphology of the MRBs was examined using scanning electron microscopy (SEM). Dried sample powder was coated with a thin layer of palladium gold alloy and imaged in a SEM instrument (Vega-Tescan, Czech Republic). Transmission electron microscopy (TEM) micrographs were recorded with a Philips CM10 (UK) operating at 60 kV tension. The X-ray diffraction (XRD) patterns of the samples were also recorded using a Siemens D-500 X-ray diffractometer with wavelength  $\lambda = 1.54\text{\AA}$  ( $\text{Cu-K}\alpha$ ), at a tube voltage of 35 kV, and tube current

of 30 mA. The magnetization was measured at room temperature with a vibrating sample magnetometer (VSM; Model 7400, Lakeshore Company, USA) and its measurement range was  $\pm 10.0$  kOe.

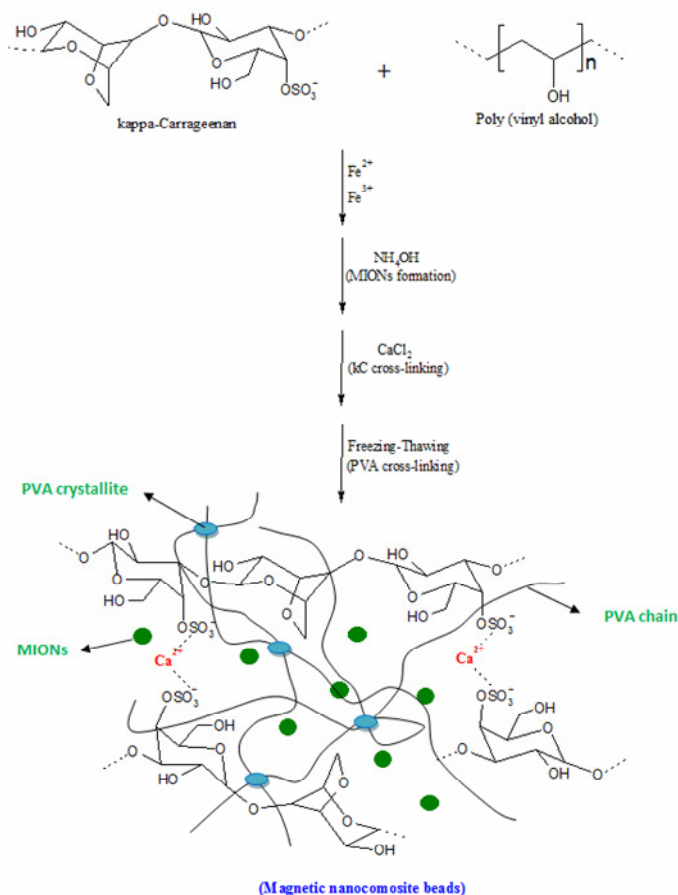
## RESULTS AND DISCUSSION

### Synthesis and characterization of beads

The synthetic mechanism of MRBs *via* the *in situ* coprecipitation of iron ions in alkaline solution are shown in Scheme 1. Firstly, iron salts were added to the *kappa*-carrageenan and poly(vinyl alcohol) structures. Then, by simultaneous additions of  $\text{NH}_4\text{OH}$  and  $\text{CaCl}_2$ , the formation of MIONs and cross-linking points between  $\kappa\text{C}$  chains occurred, which not only leads to uniform growth and dispersion of MIONs, but also causes the MIONs to be stable in the synthesized magnetic beads. Finally, the PVA chains were crosslinked using the freezing-

thawing method. The freeze-thaw process is one of the effective physical methods to produce PVA networks. In this simple crosslinking method, neither toxic chemicals nor high temperature are required. By repeating the freezing-thawing cycles, the resulting MRBs are strong and non-toxic, and thus have various applications.

FTIR spectra for MIONs,  $\kappa\text{C}$ , PVA, and MRBs are shown in Figure 1. The MIONs showed an adsorption band at  $578\text{ cm}^{-1}$ , which is attributed to the stretching of Fe-O in  $\text{Fe}_3\text{O}_4$  nanoparticles (Fig. 1a). In the spectrum of  $\kappa\text{C}$  (Fig. 1b), the bands observed at 846, 922, 1043 and  $1355\text{ cm}^{-1}$  can be attributed to the D-galactose-4-sulfate, 3,6-anhydro-D-galactose, glycosidic linkage and ester sulfate stretching of  $\kappa\text{C}$ , respectively. The broad band at  $3200\text{--}3400\text{ cm}^{-1}$  is due to stretching of the  $-\text{OH}$  groups of the substrate.



Scheme 1: Proposed mechanistic pathway for synthesis of  $\kappa\text{C}$ /PVA-based MRBs

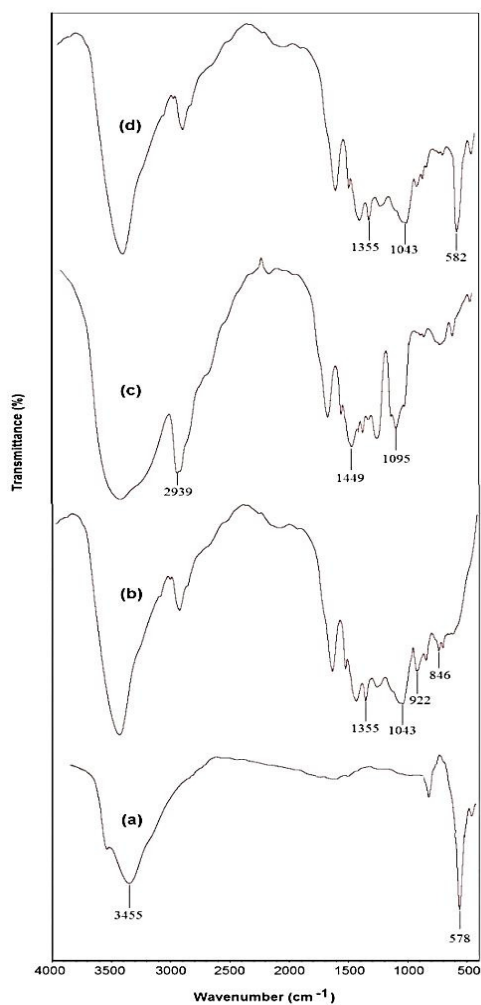


Figure 1: FTIR spectra of MIONs (a),  $\kappa$ C (b), PVA (c) and MRBs (d)

The FTIR spectrum of pure PVA (Fig. 1c) included the C-O stretching band at around  $1095\text{ cm}^{-1}$ , the C-C stretching band at around  $1449\text{ cm}^{-1}$ , the C-H stretching band at around  $2939\text{ cm}^{-1}$  and the broad O-H stretching band at around  $3200\text{--}3600\text{ cm}^{-1}$ . The MRB product comprises crosslinked  $\kappa$ C and PVA backbones incorporated in MIONs (Fig. 1d). Compared to the pristine and net MIONs,  $\kappa$ C and PVA, the intensity of some of the stretching bands in the MRBs was diminished, which demonstrated the hydrogen bonding formation and crosslinking between these groups. Also, the bond at around  $582\text{ cm}^{-1}$  confirmed the presence of MIONs in the structure of the MRB samples. In brief, the FTIR analysis revealed that the introduction of MIONs into  $\kappa$ C and PVA chains caused some interactions between the MIONs and functional groups on polymers.

In order to study the crystallographic nature of the synthesized MRBs, the XRD patterns were recorded, as shown in Figure 2. In the case of MIONs (Fig. 2a), characteristic peaks at  $2\theta=31.8, 36.7, 42.3, 57.8$  and  $63.7^\circ$  are consistent with the primary diffraction of (220), (311), (400), (511) and (440) planes of  $\text{Fe}_3\text{O}_4$  nanoparticles.<sup>33</sup> These peaks were also observed for the MRBs in Figure 3b, which indicates the formation of the spinel structure of MIONs in the bead samples. Moreover, the well-defined XRD patterns demonstrate the formation of highly crystalline MIONs. In addition, the wide peak at  $2\theta=18.8^\circ$  is attributed to the characteristic peak of PVA, confirming the semicrystalline properties of the PVA substrate.<sup>12</sup> We also used the Debye-Scherrer formula (Eq. 3) for calculating the mean grain size (D) of MRBs from XRD patterns:

$$D = \frac{k\lambda}{\beta \cos \theta} \quad (3)$$

Where  $k$  is the Scherrer constant (0.89),  $\lambda$  is the X-ray diffraction wavelength (0.1542 nm),  $\beta$  is the peak width of half maximum intensity, and  $\theta$  is the Bragg diffraction angle. According to this equation, the average crystal size for the MRBs was calculated to be 17.6 nm.

The morphology of the samples was investigated by SEM studies. Figure 3a-c shows the SEM of the net  $\kappa$ C, PVA, and MRBs. A clear and uniform surface morphology was observed for the substrates,  $\kappa$ C and PVA (Fig. 3a and b), whereas the MRB product showed a pinpoint

variation throughout the bead network (Fig. 3c). This clearly demonstrates the formation of well-defined MIONs in the bead matrixes. Moreover, the MIONs on the surface of the final product had aggregates with bigger size, which may be regulated from some  $\text{Fe}_3\text{O}_4$  nanoparticles conjoined with the neighboring particles.

The microstructure of the MRBs was revealed by TEM. As seen from Figure 3d, many MIONs with the average size of about 25 nm were homogeneously distributed on the surface of the product, which was also confirmed by SEM observation.

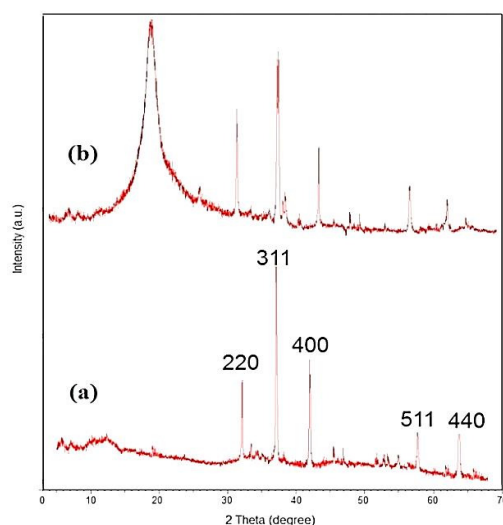


Figure 2: XRD patterns of MIONs (a) and MRBs (b)

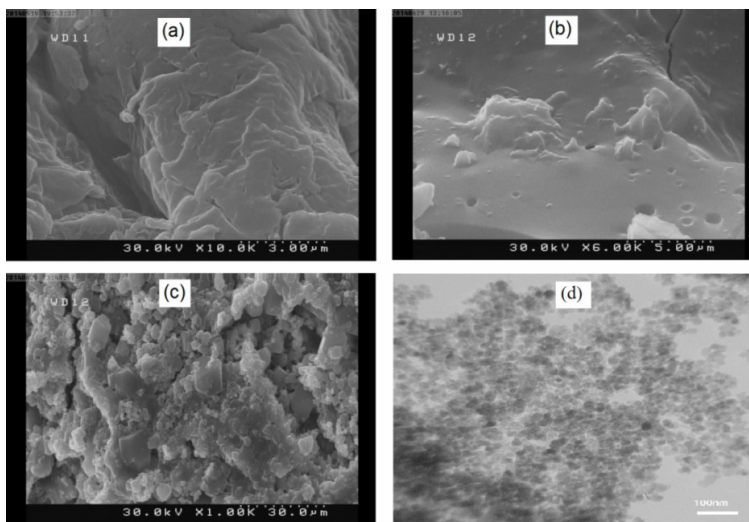


Figure 3: SEM images of the fracture surface of  $\kappa$ C (a), PVA (b) and MRBs (c); TEM image of MRBs (d)

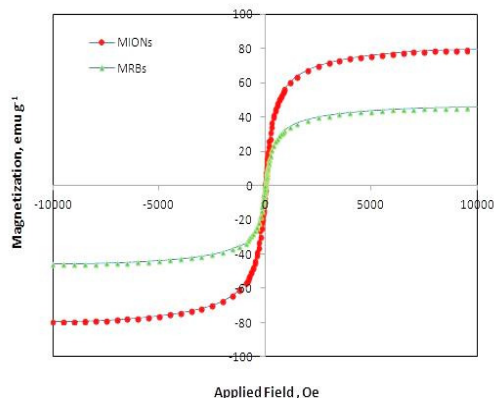


Figure 4: Magnetization curves of MIONs and MRB at 298 K

The superparamagnetic property and high saturation magnetization ( $M_s$ ) values are two important parameters for an ideal magnetic targeted drug delivery system. So, the magnetic properties of the samples were measured by using a Vibrating Sample Magnetometer (VSM). Figure 4 shows the VSM of MIONs and the resulted MRBs. The specific  $M_s$  values of MIONs and MRBs were found to be about 79.2 and 45.6 emu/g, respectively. The decrease in  $M_s$  value of MRBs confirms that the MIONs are successfully coated by the beads. In fact, this behavior is only due to the electron exchange between the surfaces of Fe atoms with the MRBs.<sup>34</sup> Meanwhile, neither coercivity nor remanence was observed for the magnetization curves of both MIONs and MRBs. It exhibits that the MRBs have a typical superparamagnetic behavior and demonstrates that they are suitable candidates for controlled magnetic drug delivery.

#### DOX loading studies

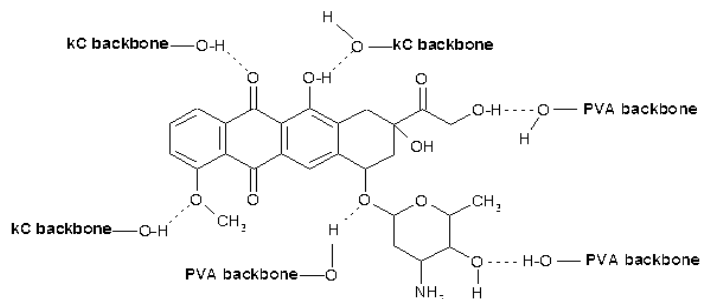
In general, the loading efficiency (LE) of the drug delivery systems is a very important parameter in practical applications. So, in this series of experiments, we investigated the LE% of the drug nanocarriers. The cross-linking density of MRBs, contact time and initial drug concentration are key factors affecting LE%, their effects have been studied and shown in Figure 5. It should be firstly noted that the main attractive interaction between DOX molecules and the synthesized MRBs is hydrogen bonding. The

hydrogen atom in  $\kappa$ C and PVA would interact with the oxygen atom in the carbonyl groups of DOX, and the hydrogen atom in the glycosidic groups of DOX would also interact with the oxygen atom in the  $\kappa$ C and PVA moieties of MRBs, as simply shown in Scheme 2.

The effect of the initial concentration of DOX on LE% is shown in Figure 5a. As can be seen from the figure, an increase in drug concentration in the swelling medium increased the amount of adsorbed DOX, as observed in many studies.<sup>35-37</sup> It is obvious that an increase in the concentration of the drug in the bead system will increase the LE% values.

The amount of the loaded drug in MRBs was also significantly affected by the contact time (Fig.5b). It is obvious that with increasing the loading time, the amount of DOX loaded is initially increased and then begins to level off. The initial increment in the amounts of the loaded drug can be attributed to the increased DOX diffusion into the swollen matrix. The most efficient time of loading was 60 min, where a major amount of drug was entrapped.

Figure 5b also shows the effect of the freezing-thawing treatment on LE% of DOX into MRBs. It was previously reported that the treatment of repeated freezing and thawing could greatly increase the cross-linking density of PVA chains.<sup>38,39</sup> Therefore, it is expected that the this method can enhance the DOX loading efficiency of MRBs. Generally, our study demonstrated that the MRBs exhibited a high LE% (above 80%).



Scheme 2: Hydrogen bond formation between functional groups of DOX molecules and substrate backbones of MRBs

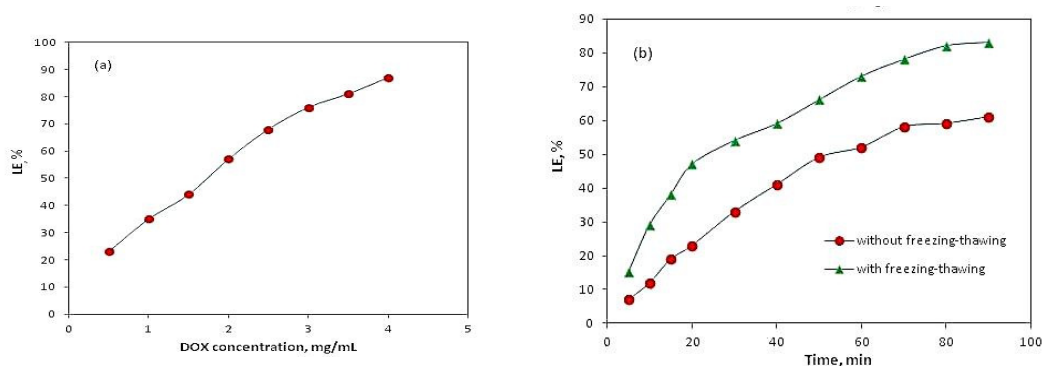


Figure 5: Effect of initial DOX concentration (a) and contact time (b) on LE% of MRBs

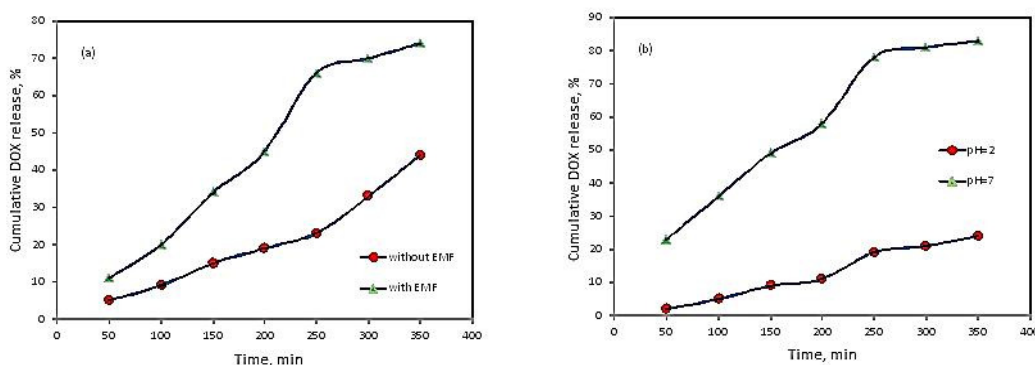


Figure 6: DOX release profiles of MRBs with and without applying magnetic field (a) and at different pH values (b) at 37 °C

### DOX releasing studies

The release profiles of DOX from the MRBs are shown in Figure 6. Because the MRBs have unique magnetic responsibility, we first investigated the DOX release behavior under an external magnetic field (EMF). As can be clearly observed from Figure 6a, employing an EMF improved the amount and the rate of DOX release from MRBs. The results can be explained by the fact that the EMF expands the MRB networks, which allows a higher number of DOX molecules to be released into the medium. This behavior was similar to the results reported by Reddy *et al.* on

DOX release from gelatin-based magnetic hydrogel nanocomposites.<sup>40</sup>

The controlled release of DOX from the MRBs was also investigated under different pH values (pH 2 and 7), as shown in Figure 6b. It can be seen from Figure 6b that the DOX amount and release rate were much higher at pH 7 than at pH 2. This behavior can be attributed to the higher swelling capacity of the MRBs at pH 7. In fact, the higher swelling at pH 7 was originated from the high repulsion between sulfate and hydroxyl groups in the MRB networks. In the solution with pH 2, this repulsion was shielded by the counter

ions, which resulted in lower swelling capacity. Moreover, hydrogen bond formation can be

catalyzed in acidic media.<sup>15</sup>

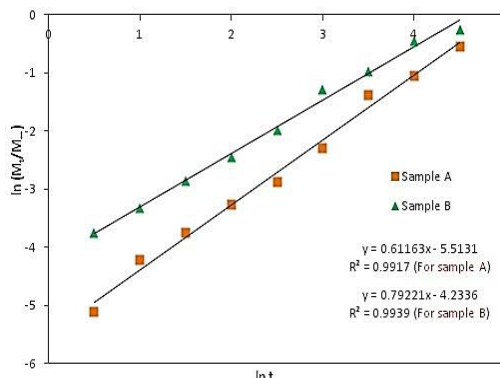


Figure 7: Fitting of data for DOX release from MRBs with various LE% for Korssemeyer-Peppas kinetic model at pH 7

Table 1  
n values of the Korssemeyer-Peppas model for the drug release mechanism

n value	Release mechanism
n < 0.45	Fickian diffusion
0.45 < n < 0.89	Non-Fickian diffusion
n > 0.89	Case II (relaxational) transport

Table 2  
Constant k and n values and correlation coefficients (R<sup>2</sup>) calculated from the Korssemeyer-Peppas equation for DOX release profiles

MRB sample	K	n	R <sup>2</sup>
Sample A (LE = 65%)	0.84	0.61	0.9917
Sample B (LE = 82%)	0.53	0.79	0.9939

To study thoroughly the DOX release behaviors of the MRBs, the release results were also analyzed using the classic Korssemeyer-Peppas<sup>41</sup> model to gain an insight into the release mechanism:

$$\ln\left(\frac{M_t}{M_\infty}\right) = \ln k + n \ln t \tag{4}$$

where  $M_t$  is the amount of drug released at time  $t$ ,  $M_\infty$  is the amount of drug released at equilibrium,  $k$  is a constant incorporating structural and geometric characteristics of the drug delivery system, and  $n$  is a characteristic exponent. In fact, the  $n$  value describes the mechanism of drug release, as summarized in Table 1.

According to Eq. 3, the values of  $k$  and  $n$  can be found from the plots of  $\ln(M_t/M_\infty)$  versus  $\ln t$  (Fig. 7). The  $k$  and  $n$  values along with the corresponding coefficients of determination ( $R^2$ ) are listed in Table 2. Firstly, the experimental data fitted well the Korssemeyer-Peppas model, as  $R^2$  was greater than 0.99 for the DOX release

profiles. In addition, the  $n$  values for the drug release from both samples A and B with various LE% are greater than 0.45 and smaller than 0.89, indicating that the DOX release follows a non-Fickian mechanism or is an anomalous release. In other words, the drug release process is well in accordance with both diffusion and polymer relaxation controlled mechanisms.<sup>42</sup>

## CONCLUSION

In conclusion, we successfully synthesized new magnetic nanocarriers by simultaneous formation of MIONs and biodegradable polymer networks in a simple and effective one-pot method. The instrumental analysis by using FTIR, SEM, TEM, XRD and VSM techniques confirmed the formation of magnetic nanoparticles within the bead network structure. As a model drug, DOX was effectively loaded into the nanomagnetic beads *via* optimizing drug concentration and contact time. The DOX

releasing profiles of the beads were also investigated by operating magnetic field and adjusting the pH of the solution. The findings of this work clearly highlight that the prepared MRBs exhibited both superparamagnetic and biocompatible properties, and conclusively are useful as potential candidates for tumor targeting drug delivery systems.

## REFERENCES

- <sup>1</sup> R. Duncan, *Nat. Rev. Cancer*, **6**, 688 (2006).
- <sup>2</sup> W. Zhang, Z. Zhang and Y. Zhang, *Nanoscale Res. Lett.*, **6**, 555 (2011).
- <sup>3</sup> Z. Liu, J. T. Robinson, S. M. Tabakman, K. Yang and H. Dai, *Mater. Today*, **14**, 316 (2011).
- <sup>4</sup> X. Yang, Y. Wang, X. Huang, Y. Ma, Y. Huang *et al.*, *J. Mater. Chem.*, **21**, 3448 (2011).
- <sup>5</sup> H. Vu-Quang, M. Yoo, H. Jeong, H. Lee, M. Muthiah *et al.*, *Acta Biomater.*, **7**, 3935 (2011).
- <sup>6</sup> J. Lee, M. J. Jung, Y. H. Hwang, Y. J. Lee, S. Lee *et al.*, *Biomaterials*, **33**, 4861 (2012).
- <sup>7</sup> A. Singh, F. Dilnawaz, S. Mewar, U. Sharma, N. R. Jagannathan *et al.*, *ACS Appl. Mater. Interfaces*, **3**, 842 (2011).
- <sup>8</sup> L. H. Reddy, J. Arias, J. Nicolas and P. Couvreur, *Chem. Rev.*, **112**, 5818 (2012).
- <sup>9</sup> W. Chen, N. Xu, L. Xu, L. Wang, Z. Li *et al.*, *Macromol. Rapid Commun.*, **31**, 228 (2010).
- <sup>10</sup> E. Eyiler and K. B. Walters, *Colloid. Surf. A: Physicochem. Eng. Aspects*, **444**, 321 (2014).
- <sup>11</sup> Y. Wang, A. Dong, Z. Yuan and D. Chen, *Colloid. Surf. A: Physicochem. Eng. Aspects*, **415**, 68 (2012).
- <sup>12</sup> L. Zhou, B. He and F. Zhang, *ACS Appl. Mater. Interfaces*, **4**, 192 (2012).
- <sup>13</sup> S. Yu, G. Wu, X. Gu, J. Wang, Y. Wang *et al.*, *Colloid. Surf. B: Biointerfaces*, **103**, 15 (2013).
- <sup>14</sup> A. Pourjavadi, S. H. Hosseini, M. Alizadeh and C. Bennett, *Colloid. Surf. B: Biointerfaces*, **116**, 49 (2014).
- <sup>15</sup> G. R. Bardajee and Z. Hooshyar, *Carbohydr. Polym.*, **101**, 741 (2014).
- <sup>16</sup> H. Y. Zhu, Y. Q. Fu, R. Jiang, J. Yao, L. Xiao *et al.*, *Bioresour. Technol.*, **105**, 24 (2012).
- <sup>17</sup> H. Liu, C. Wang, Q. Gao, X. Liu and Z. Tong, *Acta Biomater.*, **6**, 275 (2010).
- <sup>18</sup> Y. Liang, L. Zhang, W. Jiang and W. Li, *Chem. Phys. Chem.*, **8**, 2367 (2007).
- <sup>19</sup> Z. Y. Lu, J. Dai, X. N. Song, G. Wang and W. S. Yang, *Colloid. Surf., A*, **317**, 450 (2008).
- <sup>20</sup> R. E. Kirk and D. F. Othmer, in "Encyclopedia of Chemical Technology", edited by J. I. Kroschwitz and M. Howe-Grant, Wiley, New York, 1992, p. 942.
- <sup>21</sup> M. Takemasa, A. Chiba and M. Date, *Macromolecules*, **35**, 5595 (2002).
- <sup>22</sup> Y. A. Antonov and M. P. Goncalves, *Food Hydrocoll.*, **13**, 517 (1999).
- <sup>23</sup> J. V. Araujo, N. Davidenko, M. Danner, R. E. Cameron and S. M. Best, *J. Biomed. Mater. Res. A.*, **102**, 4415 (2014).
- <sup>24</sup> J. S. Park, J. W. Park and E. Ruckenstein, *Polymer*, **42**, 4271 (2001).
- <sup>25</sup> I. I. Muhamad, L. S. Fen, N. H. Hui and N. A. Mustapha, *Carbohydr. Polym.*, **83**, 1207 (2011).
- <sup>26</sup> M. Sirousazar, M. Kokabi and Z. M. Hassan, *J. Appl. Polym. Sci.*, **123**, 50 (2012).
- <sup>27</sup> K. H. Ip, B. H. Stuart and T. A. Ray, *Polym. Test.*, **30**, 732 (2011).
- <sup>28</sup> H. Hosseinzadeh, A. Pourjavadi, M. J. Zohuriaan-Mehr and G. R. Mahdavinia, *J. Bioact. Compat. Polym.*, **20**, 475 (2005).
- <sup>29</sup> H. Hosseinzadeh, *J. Chem. Sci.*, **122**, 651 (2010).
- <sup>30</sup> H. Hosseinzadeh, *J. Appl. Polym. Sci.*, **114**, 404 (2009).
- <sup>31</sup> G. R. Mahdavinia, S. Irvani, S. Zoroufi and H. Hosseinzadeh, *Iran. Polym. J.*, **23**, 335 (2014).
- <sup>32</sup> Y. Liu, P. Liu, Z. Su, F. Li and F. Wen, *Appl. Surf. Sci.*, **255**, 2020 (2008).
- <sup>33</sup> A. M. Lowman and N. A. Peppas, "Encyclopedia of Controlled Drug Delivery", edited by E. Mathiowitz, John Wiley & Sons, New York, 1999, pp. 397-418.
- <sup>34</sup> R. Kumar, B. S. Inbaraj and B. H. Chen, *Mater. Res. Bull.*, **45**, 1603 (2010).
- <sup>35</sup> M. Sen and A. Yakar, *Int. J. Pharm.*, **228**, 33 (2001).
- <sup>36</sup> P. Akkas, M. Sari, M. Sen and O. Guven, *Radiat. Phys. Chem.*, **55**, 717 (1999).
- <sup>37</sup> D. Saraydin, E. Karadag, H. N. Oztop and O. Guven, *Biomaterials*, **15**, 917 (1994).
- <sup>38</sup> T. Y. Liu, S. H. Hu, K. H. Liu, D. M. Liu and S. Y. Chen, *J. Control. Release*, **126**, 228 (2008).
- <sup>39</sup> T. Hatakeyama, J. Uno, C. Yamada, A. Kishi and H. Hatakeyama, *Thermochim. Acta*, **431**, 144 (2005).
- <sup>40</sup> N. Narayana Reddy, K. Varaprasad, S. Ravindra, G. V. Subba Reddy, K. M. S. Reddy *et al.*, *Colloid. Surf. A: Physicochem. Eng. Aspects*, **385**, 20 (2011).
- <sup>41</sup> L. Chen, G. Remondetto, M. Rouabhia, M. Subirade, *Biomaterials*, **29**, 3750 (2008).
- <sup>42</sup> S. H. Hu, T. Y. Liu, D. M. Liu and S. Y. Chen, *J. Control. Release*, **121**, 181 (2007).